
Fusion yield enhancement via secondary beam-target reactions in laser-cluster experiments

Received: 11 October 2025

Accepted: 7 January 2026

Published online: 17 January 2026

Cite this article as: Sim J., Lee S., Kim H. *et al.* Fusion yield enhancement via secondary beam-target reactions in laser-cluster experiments. *Sci Rep* (2026). <https://doi.org/10.1038/s41598-026-35722-z>

Jun Sim, Seongmin Lee, Hyeong-il Kim, Youhwan Noh, Jaehyun Song, Chiwan Song, Junho Won & Woosuk Bang

We are providing an unedited version of this manuscript to give early access to its findings. Before final publication, the manuscript will undergo further editing. Please note there may be errors present which affect the content, and all legal disclaimers apply.

If this paper is publishing under a Transparent Peer Review model then Peer Review reports will publish with the final article.

Fusion yield enhancement via secondary beam-target reactions in laser-cluster experiments

Jun Sim^{1,2,a}, Seongmin Lee^{1,2,a}, Hyeong-il Kim^{1,2}, Youhwan Noh^{1,2}, Jaehyun Song^{1,3}, Chiwan Song^{1,2}, Junho Won^{1,4}, Woosuk Bang^{1,2,*}

¹ Department of Physics and Photon Science, GIST, Gwangju 61005, South Korea

² Center for Relativistic Laser Science, Institute for Basic Science, Gwangju 61005, South Korea

³ Institute for Rare Isotope Science, Institute for Basic Science, Daejeon, 34000, Korea

⁴ Center for Exotic Nuclear Studies, Institute for Basic Science, Daejeon 34126, Korea

Abstract

Laser-cluster fusion offers a unique compact platform for studying nuclear reactions in the sub-100 keV regime. Here we report the first experimental demonstration of secondary beam-target DD fusion reactions in laser-cluster fusion experiments by surrounding a CD₄ cluster jet with a CD₂ foil. Deuterons accelerated to high ion temperatures of 60–100 keV through Coulomb explosion interacted with the surrounding CD₂ target, enhancing neutron yields by up to a factor of 3.5 compared with the cluster-only case. This enhancement was quantitatively reproduced by a time-resolved model, confirming the effectiveness of the additional target. Our results demonstrate a practical route to boost neutron production and to establish laser-cluster fusion as a compact platform for investigating a wider range of fusion reactions and cross-sections relevant to astrophysics.

^{a)}These authors contributed equally: Jun Sim, Seongmin Lee.

* Corresponding author: Woosuk Bang; E-mail: wbang@gist.ac.kr.

1. INTRODUCTION

Ultrafast, high-power laser systems have enabled experimental studies of nuclear reactions under extreme conditions relevant to astrophysical environments [1,2]. Through intense fields and highly nonlinear interactions with matter, these lasers can rapidly accelerate particles within compact laboratory setups [3-5]. Beyond particle acceleration, laser-driven experiments offer distinct advantages: they enable the creation of plasmas where bare-nucleus fusion can occur [6], providing opportunities to investigate electron [7] and plasma screening effects [8]. Moreover, the short duration of laser pulses allows for precise time-of-flight (ToF) measurements [9], facilitating clear separation of reaction products from background noise and distinguishing between fusion channels with different energies [10]. Building on these capabilities, several laser-based experimental methods have been applied to study light nuclei fusion reactions [11-14].

Among various laser-based fusion approaches, laser-cluster fusion is a distinctive method in which clusters efficiently absorb laser energy, enabling the acceleration of deuterium ions to fusion-relevant energies [15]. Clusters have typically been generated by cryogenically cooling deuterium gas (D_2) [16] or using deuterated methane (CD_4) at room temperature [17]. When irradiated by an intense laser pulse, the clusters ionize and undergo Coulomb explosion, accelerating deuterium ions to a Maxwellian-like energy distribution [18] with ion temperatures exceeding tens of keV [19-21]. The energetic ions produced in this process drive DD fusion reactions, generating 2.45 MeV neutrons emitted as few-nanosecond pulses [22]. These in-target reactions include both beam-beam fusion ($BB_{cluster}$), where energetic ions collide within the plasma, and beam-target fusion ($BT_{cluster}$), involving interactions between energetic ions and deuterium atoms or stationary ions [23,24].

Beyond these in-target reactions, energetic ions escaping from the fusion plasma can induce additional beam-target fusion in an external medium ($BT_{additional}$). Employing such a secondary target not only enhances the overall neutron yield but also enables access to a broader range of nuclear reactions depending on the target composition. Laser-cluster fusion experiments have also been demonstrated as a potential method for investigating fusion reactions in the low-

energy regime, including astrophysically relevant conditions [6]. This suggests that laser-cluster fusion can provide access to low-energy fusion cross sections for a broader range of reaction channels beyond DD fusion, when combined with a secondary target. The effectiveness of $BT_{\text{additional}}$ strongly depends on the ion temperature: higher ion temperatures increase the fusion cross section and therefore the neutron yield per ion, but at fixed laser pulse energy this also means that the total number of energetic ions is reduced. To date, theoretical investigations of $BT_{\text{additional}}$ have been limited, with one study modeling neutron yields from a deuterated polyethylene (CD_2) foil by varying cluster size [25]. However, no corresponding experimental demonstration has been reported, and a systematic and quantitative assessment of the yield enhancement achievable with an additional target remains to be carried out, motivating the present study.

In this study, we experimentally demonstrate the secondary beam-target fusion reactions induced by energetic deuterons interacting with a solid CD_2 foil in laser-cluster fusion experiments. While CD_2 serves as an effective target material for enhancing neutron production, the same approach could enable access to other reaction channels by employing alternative target compositions. This work highlights the potential of laser-cluster fusion as a compact platform for exploring a broader range of nuclear reactions relevant to astrophysics, while also establishing a practical route for boosting neutron yields.

2. EXPERIMENTAL SETUP

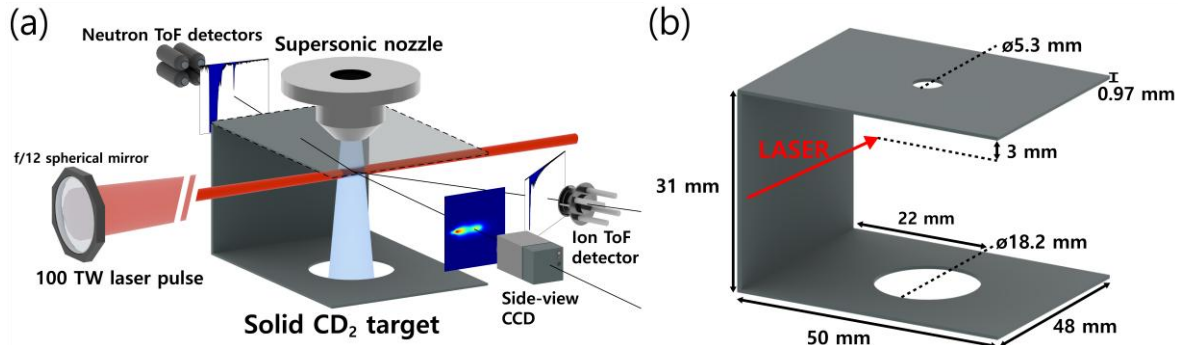


Figure 1. (a) Schematic of the experimental setup. The C-shaped CD_2 target was positioned to surround the cluster jet and fusion plasma. Ion and neutron ToF detectors, together with a

side-view CCD, were employed for diagnostics. (b) Dimensional layout of the CD₂ target, indicating the laser propagation direction and aperture sizes for the cluster jet.

The experimental configuration is illustrated in Fig. 1(a). Experiments were performed using a Ti:sapphire laser system at CoReLS, operating at a central wavelength of 800 nm with a pulse duration of 25 fs (full width at half maximum, FWHM) and a pulse energy of 2.9 J after compression. The laser beam was first reflected by a holed mirror with a 2-cm-diameter hole and then focused by an f/12 spherical mirror (focal length of 0.75 m). The beam, after a ~12% energy loss at the holed mirror, was focused to a spot size of 26 μm (FWHM), corresponding to a peak laser intensity of $1.2 \times 10^{19} \text{ W/cm}^2$. The clusters were irradiated by the focused laser beam, and the incident laser intensity was adjusted by translating the spherical mirror along the laser axis.

The clusters were generated using CD₄ gas cooled to $-41 \pm 3.0^\circ\text{C}$ and expanded through a supersonic nozzle with a throat diameter of 0.79 mm, a 5° opening angle, and an exit diameter of 5 mm, under a backing pressure of 55.5 ± 2.3 bar. Under these conditions, the average atomic number density of deuterium at the interaction region was estimated to be $(9.8 \pm 5.2) \times 10^{18} \text{ cm}^{-3}$. This estimate was obtained from Mach-Zehnder interferometer measurements, assuming the absence of monomers. Plasma emission was imaged from the side using a long-distance video microscope (Infinity K2/DistamaxTM) coupled to a Pixelfly CCD camera, oriented perpendicular to both the laser and nozzle axes.

Ion temperature and neutron yield were characterized using ToF techniques. Ion energy spectra were measured with a microchannel plate (MCP) placed 2 m from the nozzle at an angle of 67.5° with respect to the laser propagation direction. The MCP response was assumed constant, and under this assumption the measured spectra exhibited a Maxwellian-like shape with ion temperatures in the range of 60–100 keV. The MCP ToF data were grouped into 60 ± 10 keV, 80 ± 10 keV, and 100 ± 10 keV intervals. Fusion neutrons were detected using four neutron ToF detectors, each consisting of a cylindrical plastic scintillator (BC-422Q, 2 cm diameter \times 2 cm height) coupled to a photomultiplier tube (PMT) assembly (Hamamatsu H6410), positioned 3.13 m from the nozzle. The 2.45 MeV single-neutron pulse area for each

PMT was determined by averaging signals above a 0.25 V threshold over multiple campaigns and correcting for sub-threshold events using GEANT4 Monte Carlo simulations [26]. The scintillation probability, corrected for the PMT quantum efficiency, was determined from the same GEANT4 simulations to be 33.2%.

Figure 1(b) illustrates the configuration of the CD₂ target, which was fabricated to surround the plasma interaction region. The target was prepared by coating high-purity CD₂ powder (98 atom % D, Sigma-Aldrich) onto a 50 μm -thick black aluminum foil substrate. To ensure uniformity, the foil was molded into a shallow tray, and the powder was spread onto the surface of the distilled water. After evaporation on a hot plate, the remaining powder-coated substrate was subsequently heated to the melting point of CD₂. This process led to the formation of a nearly uniform solid layer upon resolidification, with a final thickness of 0.97 ± 0.14 mm. The target was designed to avoid obstructing the laser, the ion detection path to the MCP, and the gas jet flow. The deuterium atomic number density in the CD₂ target was assumed to be $n_{\text{d,target}} = 7.95 \times 10^{22} \text{ cm}^{-3}$. The average distance from the plasma to the CD₂ target was approximately 3 cm, and the target subtended 55% of the full 4π steradians.

3. NEUTRON YIELD MODEL

For quantitative analysis, theoretical neutron yields were calculated using the symmetrically expanding cylindrical fusion plasma model [23,27]. The in-target fusion neutron yield, Y_{cluster} , was calculated as

$$Y_{\text{cluster}} = \frac{N_{\text{ion}}^2}{2} \int \langle \sigma v \rangle_{kT(t)} \frac{1}{V(t)} dt + N_{\text{ion}} n_{\text{d}} \int \langle \sigma \rangle_{kT(t)/2} v_{\text{avg}}(t) \frac{V_{\text{cold}}(t)}{V(t)} dt, \quad (1)$$

where N_{ion} is the total number of ions, n_{d} is the atomic number density of deuterium in the background gas, $v_{\text{avg}}(t)$ is the average ion velocity, $\langle \sigma \rangle_{kT(t)/2}$ is the average fusion cross section, and $\langle \sigma v \rangle_{kT(t)}$ is the fusion reactivity. All reaction rates were evaluated assuming a Maxwellian ion energy distribution with ion temperature $kT(t)$, which decreases over time as energetic ions lose kinetic energy while passing through the cold background gas. The fusion cross section was taken from previously parameterized data [28]. The total plasma volume $V(t)$ was modeled

to expand at $v_{\text{avg}}(t)$, and $V_{\text{cold}}(t)$ denotes the plasma volume overlapping with the cold background gas jet.

The first term in Eq. (1) represents BB_{cluster} and is divided by two because the interacting particles are identical. The second term corresponds to BT_{cluster} , where energetic deuterium ions interact with stationary deuterium ions or atoms, and the effective ion temperature in the center-of-mass frame is taken as $kT(t)/2$. To calculate the theoretical yield, n_d was obtained from the measurements, while $V(t)$ was determined using the cylindrical fusion plasma model [23,27]. In contrast, N_{ion} was not measured experimentally and was instead adjusted as a fitting parameter to reproduce the measured yields, assuming a fixed laser-to-ion energy conversion efficiency. Our calculations confirmed that BT_{cluster} was the dominant contribution to Y_{cluster} at these high ion temperatures, consistent with previous studies [27].

The additional yield $Y_{\text{additional}}$ from the CD_2 target was evaluated by combining the Maxwellian ion energy distribution with the average number of neutrons produced per ion at the corresponding incident energy. For an incident ion energy E_{in} , the average number of neutrons per ion, $P_{\text{fusion}}(E_{\text{in}})$, is expressed as

$$P_{\text{fusion}}(E_{\text{in}}) = \int_0^{E_{\text{in}}} n_{d,\text{target}} \frac{\sigma(E/2)}{S(E)} dE, \quad (2)$$

where $n_{d,\text{target}}$ is the deuterium atomic number density within the CD_2 target and $S(E)$ is the stopping power of the CD_2 target for an ion energy E . The stopping power data were obtained from the Monte-Carlo simulation code SRIM [29]. Because the CD_2 target thickness exceeded the ion range, ions could not penetrate the target, and the integration limit was therefore set from 0 to E_{in} . For the numerical calculations, the integration started at 0.1 keV. The $Y_{\text{additional}}$ was obtained by integrating $P_{\text{fusion}}(E_{\text{in}})$ over the ion energy distribution determined by the exit ion temperature from the cluster jet, as given in Eq. (1), and scaled by a factor of 0.55 to account for the fraction of ions interacting with the CD_2 target. The total neutron yield with the CD_2 target was expressed as $Y_{\text{cluster}} + Y_{\text{additional}}$.

4. RESULTS AND DISCUSSION

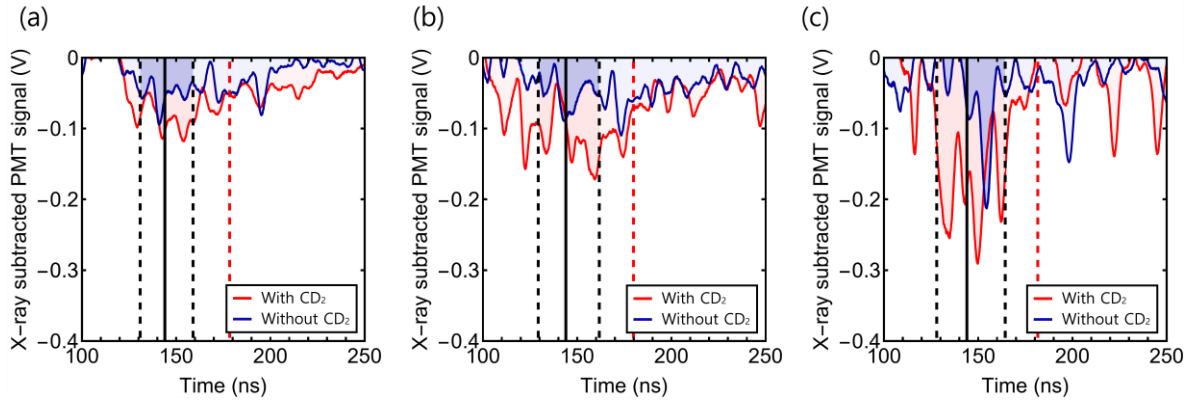


Figure 2. Average neutron ToF signals measured by PMTs after X-ray subtraction at ion temperatures of (a) 60 keV, (b) 80 keV, and (c) 100 keV. The red and blue solid lines show the averaged PMT signals with and without the CD_2 target, respectively. Black solid vertical lines indicate the ToF of 2.45 MeV fusion neutrons, while black dashed vertical lines indicate the corresponding ToF window due to Doppler broadening. Red dashed vertical lines represent the extended time window due to the CD_2 target. Time zero corresponds to the onset of X-ray emission.

Figure 2 shows averaged neutron ToF signals measured with four PMTs at ion temperatures of 60 keV, 80 keV, and 100 keV, after subtracting X-ray peaks. The subtraction was performed by fitting the early-time portion of the PMT signals with a double-exponential decay function that accounts for both fast and slow decaying components. Signals from each PMT were normalized and grouped by ion temperature. For measurements with and without the CD_2 target, the average number of laser shots was 65, 32, and 38 at 60 keV, 80 keV, and 100 keV, respectively.

The calculated ToF of 2.45 MeV neutrons from the target chamber center (TCC) was 144 ns (black solid lines). To define the in-target ToF windows, the neutron energy spread owing to Doppler broadening [30] was taken into account. The interaction time for ions with average kinetic energy traversing the cluster jet was also considered but found to be less than 1 ns, which is much shorter than the Doppler-broadened window. The combined effects are shown by the black dashed lines in Fig. 2, corresponding to widths of 28 ns, 32 ns, and 36 ns for ion temperatures of 60 keV, 80 keV, and 100 keV, respectively. Signals after the ToF window were excluded as scattered components, while early-arriving signals were excluded as residuals from the X-ray subtraction.

When the CD_2 target was placed, $BT_{\text{additional}}$ neutrons could arrive after the ToF window defined for the in-target fusion. To account for this, the window was extended by adding the estimated ion flight time from the TCC to the CD_2 target, calculated using the average ion energy derived from the measured temperature. An additional 10 ns margin was included to account for ions near the most probable energy. The resultant total extensions were 20 ns, 19 ns, and 18 ns to the original time window for ion temperatures of 60 keV, 80 keV, and 100 keV, respectively (red dashed lines). This procedure enabled separation of fusion neutrons from scattered components and revealed a systematic increase in neutron signals with ion temperature in both cases with and without the CD_2 target.

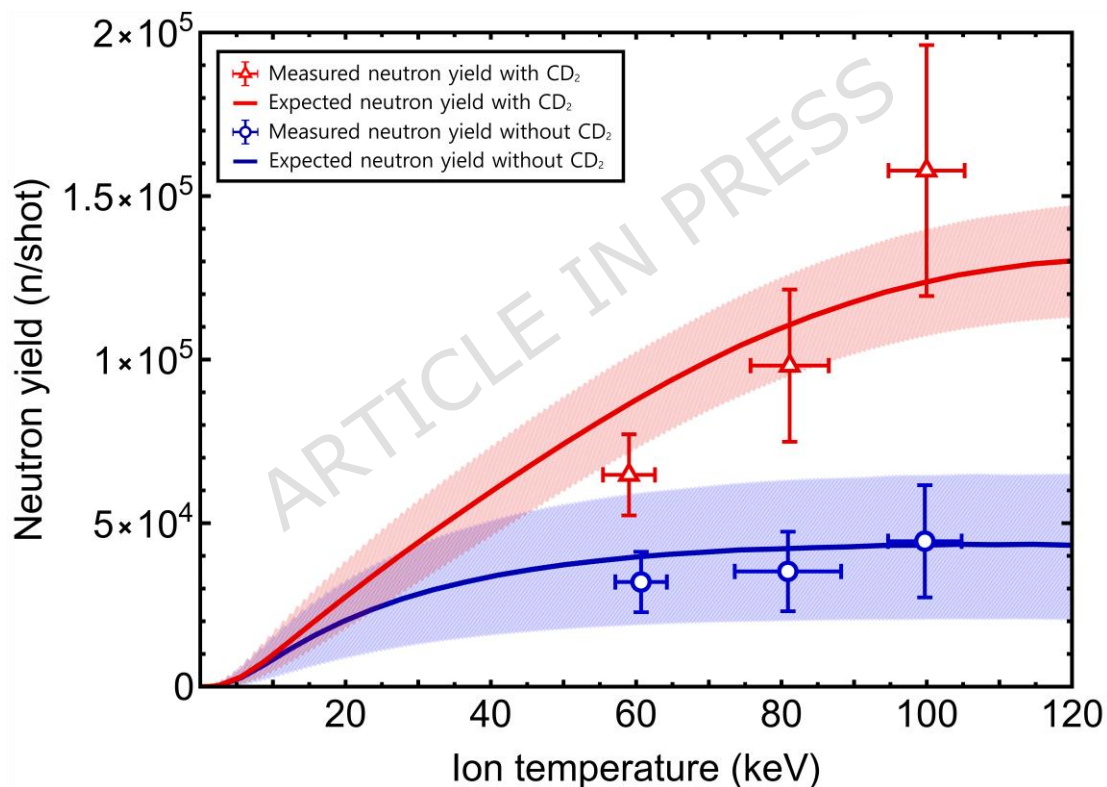


Figure 3. Experimentally measured neutron yields and theoretical yield curves as functions of ion temperature for both cases, with and without the CD_2 target. Hollow blue circles denote neutron yields from in-target fusion, while hollow red triangles denote neutron yields including additional fusion due to the CD_2 target. Vertical error bars represent the standard errors of the average neutron yields, determined from repeated shots at 60 keV, 80 keV, and 100 keV. Horizontal error bars indicate the standard deviations of the grouped ion temperatures. Red and blue solid lines represent the theoretical yield curves with and without the CD_2 target, respectively, and are scaled to fit the measurements. The shaded regions reflect the uncertainty in the background deuterium atomic number density in the model predictions.

Figure 3 shows the measured neutron yields with and without the CD_2 target alongside the corresponding model predictions. To obtain the yields, the number of neutrons detected at the scintillator was first estimated by dividing the PMT signal area by the single-neutron pulse area. These values were then converted to the average neutron yield per shot after accounting for detection probability and geometrical scaling, assuming isotropic neutron emission (See Supplementary Fig. S1 for details). For the yields without the CD_2 target, signals only within the in-target windows were taken into account. The resulting neutron yields were 3.2×10^4 , 3.5×10^4 , and 4.4×10^4 neutrons per shot at ion temperatures of 61 ± 3.6 keV, 81 ± 7.3 keV, and 100 ± 5.1 keV, respectively.

The neutron yields with the CD_2 target were measured using the extended ToF windows shown in Fig. 2, with background correction applied by subtracting the signals obtained without the CD_2 target over the same time interval. The resulting yields were 6.5×10^4 , 9.8×10^4 , and 1.6×10^5 neutrons per shot at the ion temperatures of 59 ± 3.6 keV, 81 ± 5.4 keV, and 100 ± 5.2 keV, respectively. While the extended ToF windows were used, the majority of the neutron signals still originated from the in-target ToF windows. This is because the windows for the in-target and additional target largely overlap.

The model was fitted to the measured yields both with and without the CD_2 target, and it successfully reproduced the experimentally observed trend of increasing neutron yield with ion temperature. The shaded regions surrounding the red and blue curves in Fig. 3 indicate the uncertainty in the measured deuterium gas atomic number density, $n_d = (9.8 \pm 5.2) \times 10^{18} \text{ cm}^{-3}$. For each curve, the upper and lower edges of the shaded region correspond to the upper and lower bounds of n_d , respectively. The model further indicates that the total neutron yield increases with deuterium atomic number density.

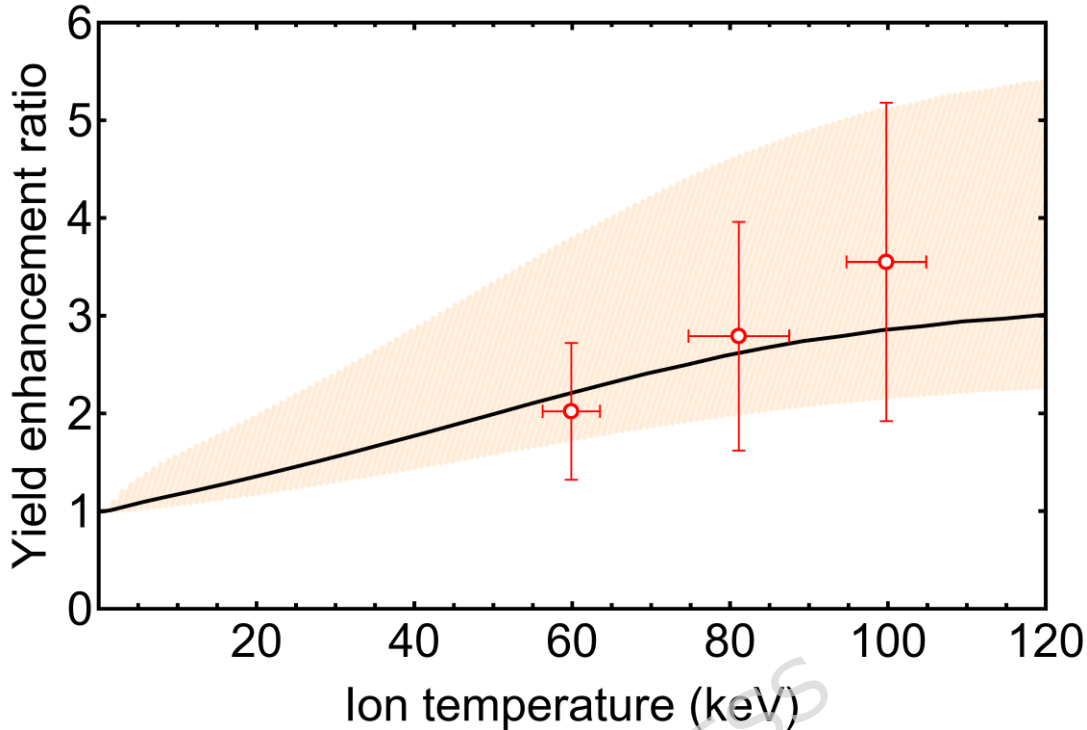


Figure 4. Fusion yield enhancement ratio due to the CD_2 target as a function of ion temperature. Hollow red circles and error bars are obtained from the experimental measurements. The black solid line indicates the enhancement ratio estimated by the model. The shaded region around the model represents the uncertainty range in the deuterium atomic number density.

Figure 4 shows the fusion yield enhancement ratios $(Y_{\text{cluster}} + Y_{\text{additional}}) / Y_{\text{cluster}}$, obtained from Fig. 3. These are compared with theoretical model predictions. The neutron yield was amplified by factors of 2.0, 2.8, and 3.5 at ion temperatures of 60 ± 3.6 keV, 81 ± 6.4 keV, and 100 ± 5.1 keV, respectively (hollow red circles). A full 4π enclosure of the cluster jet by the CD_2 target would increase the corresponding ratios to 2.9, 4.3, and 5.6. Vertical error bars represent statistical uncertainties of the yield enhancement ratio, obtained from standard error propagation of the individual yields in Fig. 3. Horizontal error bars represent the standard deviations of the grouped ion temperatures.

The enhancement ratio exhibits a nearly linear dependence on ion temperature up to about 100 keV at a fixed deuterium atomic number density, as predicted by the symmetrically expanding cylindrical plasma model (black solid lines). This ratio can be directly compared with the experimental results because the fitted parameter N_{ion} cancels in the ratio. The model predictions fall within the bounds defined by the uncertainty of the deuterium atomic number

density (shaded region), which directly reflects the uncertainty in the deuterium density input to the model. The lower bound of the shaded region corresponds to yield ratios at higher deuterium atomic densities, where an increase in Y_{cluster} , combined with a decrease in $Y_{\text{additional}}$, leads to a lower yield ratio.

Our results clearly demonstrate that the ratio of $BT_{\text{additional}}$ to BT_{cluster} reactions depends on both the ion temperature and the deuterium atomic number density in the cluster jet. Because Y_{cluster} can be estimated in advance, our analysis provides a useful guideline for predicting $Y_{\text{additional}}$ and extending this approach to other beam-target reactions in experimental design.

5. CONCLUSION

For the first time, we experimentally demonstrated secondary beam-target fusion reactions induced by energetic deuterium ions interacting with the surrounding CD_2 target in laser-cluster fusion experiments. High ion temperatures of up to 100 keV were achieved using cooled CD_4 cluster jets, and a clear enhancement of fusion neutron yield was observed with the CD_2 target. The measured fusion yields showed good agreement with theoretical predictions. Importantly, the theoretical model accurately reproduced the observed dependence of the fusion yield enhancement ratio on ion temperature.

In addition to enhancing fusion yields, this approach can be extended to explore a wider range of nuclear reactions by employing different target materials. It also provides a complementary experimental platform for studying low-energy fusion cross sections relevant to astrophysics, while retaining the inherent advantages of laser-cluster fusion. In this broader context, recent advances in high-power laser facilities have stimulated active research on both in-target and beam-target nuclear reactions, mostly at ion energies above 100 keV. Our results provide a valuable reference for extending such investigations into the sub-100 keV regime and open opportunities for low-energy fusion cross-section measurements.

Data availability

The data that support the findings of this study are available from the corresponding author upon reasonable request.

Funding

This work was supported by the National Research Foundation of Korea (NRF) grant funded by the Korea government (MSIT) (No. RS-2023-NR076370). In part, this work was supported by the Institute for Basic Science under IBS-R038-D1 and by the NRF grant No. RS-2023-00218180.

Author Contributions

J.S., S.L., H.K., Y.N., J.S., C.S., J.W., and W.B. designed and performed the experiments.

J.S., S.L., and J.W. performed the simulations and analyzed the data.

J.S., S.L., and W.B. wrote the manuscript. All authors reviewed the manuscript.

REFERENCES

- [1] D. T. Casey *et al.*, *Nature Physics* **13**, 1227 (2017).
- [2] J. Feng *et al.*, *Proceedings of the National Academy of Sciences* **121**, e2413221121 (2024).
- [3] M. J. V. Streeter *et al.*, *Nature Communications* **16**, 1004 (2025).
- [4] K. Pöder *et al.*, *Physical Review Letters* **132**, 195001 (2024).
- [5] E. Skopalová, Y. C. El-Taha, A. Zair, M. Hohenberger, E. Springate, J. W. G. Tisch, R. A. Smith, and J. P. Marangos, *Physical Review Letters* **104**, 203401 (2010).
- [6] M. Barbui *et al.*, *Physical Review Letters* **111**, 082502 (2013).
- [7] C. P. Berlinguet, Y.-M. Chiang, J. N. Munday, T. Schenkel, D. K. Fork, R. Koningstein, and M. D. Trevithick, *Nature* **570**, 45 (2019).
- [8] Y. Wu and A. Pálffy, *The Astrophysical Journal* **838**, 55 (2017).
- [9] W. Bang *et al.*, *Physical Review Letters* **111**, 055002 (2013).
- [10] W. Wang *et al.*, *Physics Letters B* **843**, 138034 (2023).
- [11] W. Bang *et al.*, *Physical Review E* **88**, 033108 (2013).
- [12] C. Labaune, C. Baccou, S. Depierreux, C. Goyon, G. Loisel, V. Yahia, and J. Rafelski, *Nat. Commun.* **4**, 2506 (2013).
- [13] X. Zhang *et al.*, *Physical Review C* **96**, 055801 (2017).
- [14] V. Istokskaya *et al.*, *Communications Physics* **6**, 27 (2023).
- [15] T. Ditmire, J. Zweiback, V. P. Yanovsky, T. E. Cowan, G. Hays, and K. B. Wharton, *Nature* **398**, 489 (1999).
- [16] J. Zweiback, R. A. Smith, T. E. Cowan, G. Hays, K. B. Wharton, V. P. Yanovsky, and T. Ditmire, *Physical Review Letters* **84**, 2634 (2000).
- [17] K. Madison, P. Patel, D. Price, A. Edens, M. Allen, T. Cowan, J. Zweiback, and T. Ditmire, *Physics of Plasmas* **11**, 270 (2004).
- [18] W. Bang, G. Dyer, H. J. Quevedo, A. C. Bernstein, E. Gaul, M. Donovan, and T. Ditmire, *Physical Review E* **87**, 023106 (2013).
- [19] K. W. Madison, P. K. Patel, M. Allen, D. Price, R. Fitzpatrick, and T. Ditmire, *Physical Review A* **70**, 053201 (2004).
- [20] A. R. Holkundkar, G. Mishra, and N. Gupta, *Physics of Plasmas* **21** (2014).
- [21] G. Grillon *et al.*, *Physical Review Letters* **89**, 065005 (2002).
- [22] W. Bang, G. Dyer, H. Quevedo, A. Bernstein, E. Gaul, J. Rougk, F. Aymond, M. Donovan, and T. Ditmire, *Physics of Plasmas* **20** (2013).
- [23] W. Bang, *Physical Review E* **92**, 013102 (2015).
- [24] J. Zweiback *et al.*, *Physics of Plasmas* **9**, 3108 (2002).
- [25] J. Davis, G. Petrov, and A. Velikovich, *Physics of Plasmas* **13** (2006).
- [26] S. Agostinelli *et al.*, *Nuclear instruments and methods in physics research section A: Accelerators, Spectrometers, Detectors and Associated Equipment* **506**, 250 (2003).
- [27] J. Won, J. Song, S. Lee, C. Song, and W. Bang, *Nuclear Fusion* **63**, 066031 (2023).
- [28] H.-S. Bosch and G. M. Hale, *Nuclear fusion* **32**, 611 (1992).
- [29] J. F. Ziegler, M. D. Ziegler, and J. P. Biersack, *Nuclear Instruments and Methods in Physics Research Section B: Beam Interactions with Materials and Atoms* **268**, 1818 (2010).
- [30] T. Elevant, *Nuclear Instruments and Methods in Physics Research* **185**, 313 (1981).